NUMERICAL METHOD AND ANALYSIS OF A TUBE INDIRECT EVAPORATIVE COOLER

by

Rui LI, Wenhe ZHOU**, *Jianyun WU, Jianxia LI, Xinyue DONG, and Juan ZHAO

School of Environmental and Municipal Engineering,
Lanzhou Jiaotong University, Lanzhou, China

Original scientific paper
https://doi.org/10.2298/TSCI201121198L

The tube indirect evaporative cooler is energy-saving and environmentally friendly, and its heat transfer mechanism still needs to be fully indicated, for which the numerical method is more suitable than the experiment. Because many numerical researches focusing on the tube indirect evaporative cooler are usually based on the simplified models, such as single tube model, single side model, 1-D, and 2-D model, the further improvement is still needed. Meanwhile, the tube indirect evaporative cooler is always expected to supply more cooling air with lower temperature at lower cost of energy, but many present studies are focusing on the improvement of heat transfer only and ignoring the energy cost. This paper proposed a 3-D full-scale numerical model and method verified by the experimental data, by which, the energy output (primary air-cooling capacity) and quality (temperature of primary air outlet) at the resistance loss (resistance) of the tube indirect evaporative cooler are analyzed with the help of FLUENT software.

Key words: *evaporative cooler, tube indirect evaporative cooler, numerical analysis, cooling efficiency*

Introduction

Evaporative cooler (EC) cools air by water evaporation [1, 2] at the cost of water, blower and pump only, and no chemical refrigerant involved, especially in the area with large temperature difference between dry bulb and wet bulb, such as Lanzhou of China [3, 4]. The tube indirect evaporative cooler (TIEC) is more suitable for the environment wanted lower humidity [5, 6]. Due to the complex mechanism of heat and mass transfer, the numerical method is indispensable for the performance study of TIEC.

Hettiarachchi *et al.* [7] established a 2-D numerical model based on the finite difference methods to obtain the longitudinal heat conduction and mass transfer relationship involving the secondary air and the water film of indirect evaporative cooler (IEC). Yunran *et al.* [8] used the finite difference methods to predict the energy saving potential of IEC in Hong Kong by a 2-D numerical model. Zheng *et al.* [9] established a 2-D numerical model of IEC using finite element method under the air condensation condition, and analyzed the heat and mass transfer performance of IEC. Chen *et al.* [10] established an 1-D unit model to analyze the heat and mass transfer performance of IEC and its annual operation in Hong Kong. Chengqin and Hongxing [11] analyzed the performance of IEC under various conditions in a 2-D numerical

* Corresponding author, e-mail: zwh6888@mail.lzjtu.cn

method. Moshar *et al.* [12] used a 2-D numerical model to analyze the adaptability of three IEC in six cities, and proposed a dimensionless water evaporation rate index. Cui *et al.* [13] established a numerical model using the improved logarithmic mean temperature difference method, and analyzed the relationship between the latent heat and water evaporation rate of IEC. Hao [14] verified a single tube numerical model and method of TIEC with experimental data. Min *et al.* [15, 16] established an IEC model considering air condensation under different outdoor climate conditions by a 2-D numerical method. Sun *et al.* [17] used the single tube model to study TIEC performance.

Obviously, the numerical study on TIEC performance is very scattered, especially many of which are based on the simplified models and methods such as single tube model, single side model, 1-D, and 2-D model. In order to fully indicate the heat and mass transfer mechanism of TIEC and evaluate its performance more appropriately, a 3-D model will be built and verified firstly in this paper. Then, the energy output (primary air-cooling capacity) and quality (temperature of primary air outlet) at the resistance loss (resistance) of the TIEC will be calculated and analyzed with the help of FLUENT software.

Numerical model and method

Physical model

The TIEC showed by fig. 1 is composed of 780 aluminum oval tubes arranged in 38 rows with 21 tubes in odd rows and 20 tubes in even rows, and its elliptic tubes are all 1.5 m in length, 0.025 m in long diameter, 0.02 m in short diameter, and 0.03 m in pipe spacing. The upwind dimension of primary air is 1.18 m × 0.69 m, and that of secondary air is 1.5 m × 0.69 m. The maximum volume of the primary air blower and the secondary air blower are all 10000 m^3/h and adjustable.

The heat and mass transfer process of TIEC is:

– Forced by the pump, the circulating water is sprayed on the heat exchange tubes from the water distribution device at the top of TIEC, and the water films adhere to the outer walls of the tubes.
– Forced by the secondary air blower, the secondary air (before inlet, it is ambient air) flows transversely across the heat exchange tube bundle from the bottom to the top of TIEC, whose moisture will increase continuously.
– The water film around the tube is cooled due to evaporation, and then, the heat exchange tubes are cooled.
– Forced by the primary air blower, the primary air (before inlet, it is ambient air) blows lengthwise inside the elliptic tube and is cooled [11].

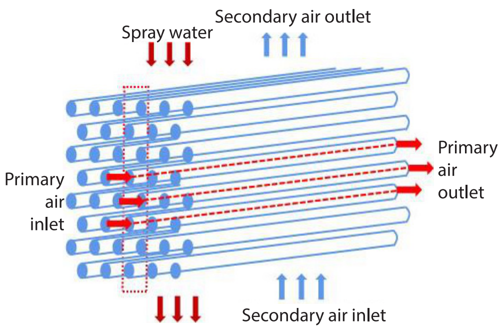

Figure 1. Schematic diagram of TIEC

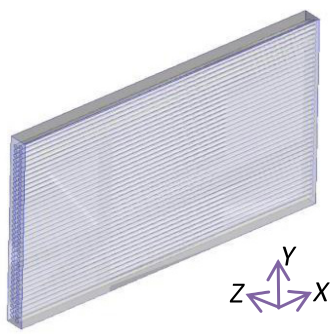

Figure 2. Physical model

Considering the symmetrical structure of TIEC and the computer resource saving, a structural unit of the TIEC is selected as the physical model shown in the red box of fig.1. As show in fig. 2, the model consists of 75 elliptical tubes. The upwind size, the flow area and the hydraulic diameter of primary air are 1.18 m × 0.065 m, 6.64 m^2 and 0.022 m, respectively. The upwind size, the flow area and the hydraulic diameter of the secondary air are 1.5 m × 0.065 m, 3.69 m^2 and 0.12 m, respectively.

Numerical model

In order to simplify the calculation, several assumptions are made:

- The heat exchange between the TIEC and the environment is ignored [18, 19].
- The air-flow is incompressible [20].
- The influence of thermal radiation is ignored.
- The water loss due to evaporation is neglected.
- The interfacial mass transfer resistance between the secondary air and the water film is ignored.
- The inlet pressure of primary and secondary air is constant and the velocity is evenly distributed.
- Lewis number is considered to be constant [21].
- The parameter change of the primary air happened along x direction only and the parameter change of the secondary air happened along y direction only.

The numerical simulation is based on the law of mass, momentum and energy-conservation, which can be expressed uniformly:

$$\frac{\partial(\rho\phi)}{\partial t} + \mathrm{div}(\rho U\phi) = \mathrm{div}(\Gamma_\phi \mathrm{grad}\phi) + S_\phi \tag{1}$$

Considering the parameter change of the primary air happened along x-direction only and the parameter change of the secondary air happened along y direction only, the energy conservation of the primary air, the moisture conservation of the secondary air and the energy conservation of the secondary air can be simply described 1-D eqs. (2)-(4).

For conservation of energy in the primary air:

$$m_1 c_1 \frac{\partial T_1}{\partial x} = h_1 \pi L_1 (T_\mathrm{w} - T_1) \tag{2}$$

For conservation of moisture in the secondary air:

$$m_2 l_2 \frac{\partial W_2}{\partial y} = k_D L_2 (W_\mathrm{w} - W_2) \tag{3}$$

For conservation of energy in the secondary air:

$$m_2 l_2 \frac{\partial i_2}{\partial y} = h_2 L_2 (T_\mathrm{w} - T_2) + L_2 i_\mathrm{g} k_D (W_\mathrm{w} - W_2) \tag{4}$$

For conservation of energy at the tube wall and the wall film:

$$h_2\left(T_\mathrm{w} - T_2\right) + h_1\left(T_\mathrm{w} - T_1\right) + k_D i_\mathrm{fg}\left(W_\mathrm{w} - W_2\right) - \left(k_\mathrm{x} d \frac{\partial^2 T_\mathrm{w}}{\partial x^2} + k_\mathrm{y} d \frac{\partial^2 T_\mathrm{w}}{\partial y^2} + k_z d \frac{\partial^2 T_\mathrm{w}}{\partial z^2}\right) = 0 \tag{5}$$

The heat transfer per unit area, q, can be given:

$$q = \frac{c m_1 \left(T_{1'} - T_{1''}\right)}{n \pi L_1 l_1} \tag{6}$$

The resistance per unit area, p, can be given:

$$p = p_p + p_{p'} + p_s \tag{7}$$

$$p_p = \lambda \frac{1}{L_\ell} \frac{\rho_\ell u_\ell^2}{2A_p} \tag{8}$$

$$p_{p'} = \zeta \frac{\rho_\ell u_\ell^2}{2A_{p'}} \tag{9}$$

$$p_2 = 1.3 \times 0.334 C_f n \frac{G_{\max}^2}{2\rho_2 A_s} \tag{10}$$

The resistance per unit area, p, is the composed of the resistance per unit area of primary air, p_p, the local resistance per unit area of primary air, and, $p_{p'}$, and the resistance per unit area of secondary air, p_s.

The thickness of water film, δ, can be given:

$$\delta = \left(\frac{3\mu_\mathrm{f} m_\mathrm{f}}{\rho_\mathrm{f}^2 \mathrm{g}} \right)^{1/3} \tag{11}$$

The cooling efficiency, η, can be given [22]:

$$\eta = \frac{T_{1'} - T_{1''}}{T_{1'} - T_\mathrm{wb}} \tag{12}$$

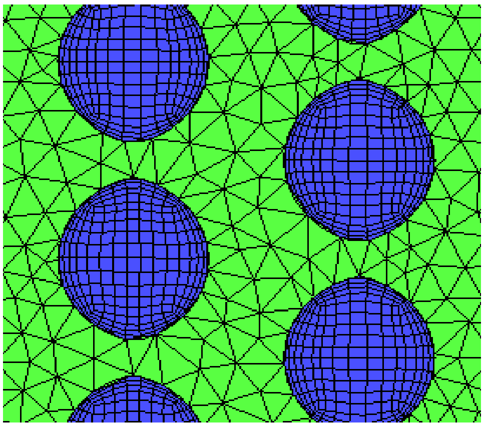

Figure 3. Mesh of the computational domain

Mesh and its independence verification

As fig. 3 shows [23], the structured grid is used to discretize the locally encrypted ellipse tubes in the model, and the unstructured grid is used in other regions which are relatively sparse. Several sets of grids are tested to select a reasonable grid number. The calculation results with three grid numbers of 3.6 million, 5.5 million, and 8.2 million are given in tab. 1, and finally, the grid of 5.5 million is selected for the numerical calculation. During the calculation, the pipe wall boundary conditions at inlet and outlet are defined as speed type and pressure type, respectively, the convergence criterion is 10^{-3}, but the energy equation is 10^{-7}, and the calculation conditions are set dry bulb temperature, wet bulb temperature and velocity at primary air inlet are 31.3 °C, 20.1 °C, and 6 m/s, respectively, and the speed of secondary air is 3 m/s.

Table 1. Result of independence verification

Number of grids	$3300 \cdot 10^3$	$5500 \cdot 10^3$	$8200 \cdot 10^3$
Outlet temperature	27.4 °C	27.5 °C	27.5 °C
Temperature drop	3.5 °C	3.4 °C	3.4 °C
Cooling efficiency	31.3%	30.4%	30.4%

Consideration of boundary-layer of primary air side

When the primary air-flows across the tube, the boundary-layer, which will deteriorate heat transfer, will be formed along the inner wall and its thickness is related to the Reynolds number. Table 2 demonstrates the calculation results of the thicknesses of the air boundary-layer corresponding to the speed of various primary air.

Table 2. Thicknesses of boundary-layer

Primary air speed [ms^{-1}]	Air density [kgm^{-3}]	Air dynamic viscosity [kgm^{-1}s^{-1}]	Length of boundary-layer [m]	$Y+$	Re of air	Thickness of boundary-layer [m]
6	1.185	$1.835 \cdot 10^{-5}$	0.073	30	$2.8 \cdot 10^{4}$	$1.2 \cdot 10^{-3}$
7	1.185	$1.835 \cdot 10^{-5}$	0.073	30	$3.3 \cdot 10^{4}$	$1.1 \cdot 10^{-3}$
8	1.185	$1.835 \cdot 10^{-5}$	0.073	30	$3.8 \cdot 10^{4}$	$9.6 \cdot 10^{-4}$
9	1.185	$1.835 \cdot 10^{-5}$	0.073	30	$4.2 \cdot 10^{4}$	$8.7 \cdot 10^{-4}$
10	1.185	$1.835 \cdot 10^{-5}$	0.073	30	$4.7 \cdot 10^{4}$	$7.9 \cdot 10^{-4}$

Although the accuracy of numerical calculation is related to the boundary-layer, the layer is usually ignored. Table 3 compares the numerical and experimental results with the boundary-layer and without the boundary-layer. The maximum error between the temperatures of primary air outlet simulated with the boundary-layer and the experimental result is 0.44 °C, and the minimum is 0.18 °C. While the maximum error between the temperatures of primary air outlet simulated without the boundary-layer and the experimental result is 0.64 °C, and the minimum is 0.24 °C. It is obvious that consideration of the boundary-layer during numerical simulation is necessary.

Table 3. Comparison of the temperatures of primary air outlet between considering boundary-layer and not

Primary air inlet temperature [°C]	Temperature of primary air outlet tested [°C]	Temperature of primary air outlet simulated with boundary-layer [°C]	Absolute error [°C]	Temperature of primary air outlet simulated without boundary-layer [°C]	Absolute error [°C]
24.7	21.8	21.98	0.18	22.04	0.24
25.0	22.0	22.24	0.24	22.09	0.29
25.4	22.1	22.36	0.26	22.48	0.38
25.8	22.3	22.61	0.31	22.72	0.42
26.3	22.4	22.84	0.44	23.04	0.64
26.9	22.8	23.08	0.28	23.23	0.43

Numerical method and its validation

With the help of FLUENT software and staggered grids, the finite volume method, SIMPLE algorithm, VOF model and relative k-ε model are used in this paper. First, the momentum equation is used to solve the velocity field. Next, the coupled solution method is used to obtain the pressure field, and then the component input model is opened. The UDF is used in order to accurately simulate the water film evaporation phenomenon outside the tube. The model formula is expressed:

$$M = 0.1\rho_2 V_2 \left| \frac{T_2 - T_q}{T_2} \right| \tag{13}$$

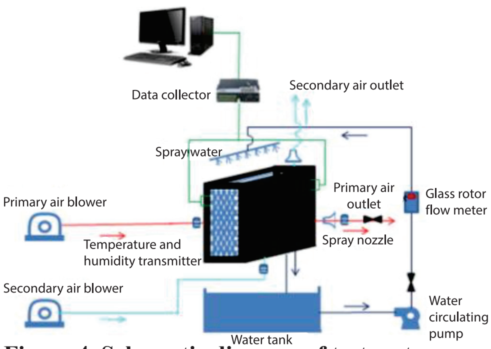

Figure 4. Schematic diagram of test system

The aforementioned TIEC was tested from 8:00 a. m. to 8:00 p. m. each day from July 24 to September 9 in 2014 by the test system showed in fig. 4. As a supplement, the numerical study was performed based on a single tube model and method by Yu [24], who belongs to our team. The test devices are shown in tab. 4 and the data acquisition frequency is 30 minutes. The test data and the numerical results are shown in figs. 5(a) and 5(b).

Table 4. Tested parameters and instruments

Parameter	Device	Number	Technical parameter
Air temperature/ humidity	Temperature and humidity transmitter	3	JWSK-6ACC02, humidity 0-100% ±2% (25°C, 5-95%RH), temperature –40-120 °C ±0.5 °C
	Wet and dry bulb thermometer	7	Range: –0.5-55 °C ±0.1 °C
Spray water temperature	Thermocouple	1	WZPK, Range: –200-500 °C ±0.1°C
Spray water rate	Glass rotor flowmeter	1	VA10-40, Range: 0.5-5 m^3/h ±0.0072 m^3/h
Primary air-flow	Nozzle flowmeter 1	3	Throat diameter:189 mm, flux coefficient: 0.95
Secondary air-flow	Nozzle flowmeter 2	4	Throat diameter:110 mm, flux coefficient: 0.95

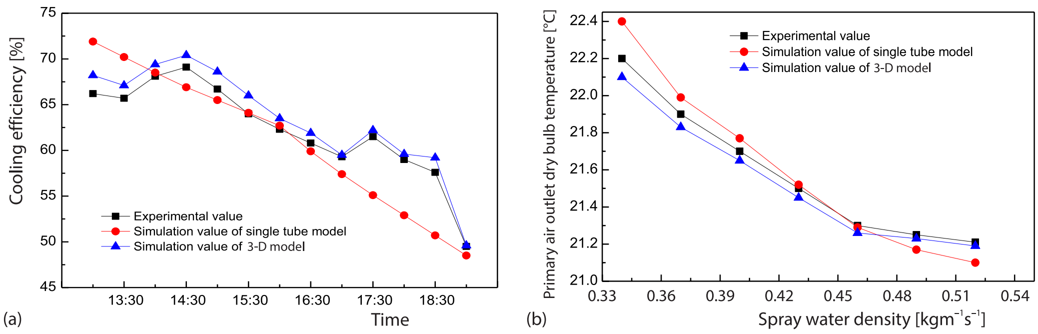

Figure 5. Comparison of the cooling efficiency and primary air outlet dry bulb temperature

The valid of the numerical model and method is shown in figs. 5(a) and 5(b). According to fig.5(a), the cooling efficiency calculated by the 3-D full-scale numerical model is closer to the experimental value than that by the single tube model, and the average absolute error of the cooling efficiency is 4.7% of the single tube model and 1.9% of the 3-D full-scale numerical model, respectively.

According to fig. 5(b), because the water film on the pipe wall would be more complete with the increase of spray water density, its evaporation is increasing too and the primary air outlet dry bulb temperature is decreasing. Until the spray water density is about 0.46 kg/m·s, the primary air outlet dry bulb temperature tends to be stable.

It is obvious that the 3-D full-scale numerical model and method proposed by this paper is more valid to predict the performance of TIEC.

Results and discussion

Table 5 shows the average values of some key parameters on August 15, 2014, which are similar to that of the summer and will be taken as the input conditions during the numerical simulation followed, Meanwhile, based on which, we obtain h_p = 32.05 W/m^{2}k, h_s = 378.06 W/m^2·k, and k_D = 0.376 kg/m^{2}s.

Table 5. Test conditions

Environmental dry bulb temperature	Environmental wet bulb temperature	Environmental relative humidity	Water temperature	Spray water density	Droplet diameter	Water film thickness
26.1°C	18.2 °C	49.04 %RH	24.3 °C	0.46 kg/ms	$2 \cdot 10^{-3}$ m	$5.03 \cdot 10^{-4}$ m

Parameter effects of working medium

Velocity effects of primary and secondary air

It is well known that when the primary air velocity is constant, the water film evaporation and latent heat transfer will be enhanced with the increase of speed of secondary air, but there will be more sensible heat of the secondary air to be balanced too. In the meantime, the contact time between the water film and the secondary air will be shortened, and the secondary air resistance and the water-drift will increase. Likewise, when the secondary air velocity is constant, more sensible heat involved will be introduced and the contact time between the tube wall and the primary air will be shortened with the increase of primary air speed, also the primary air resistance will increase. Therefore, for a certain TIEC, there must be a reasonable velocity of primary air and secondary air. For this purpose, the primary air speed of 6.5 m/s, 7 m/s, 7.5 m/s, 8 m/s, 8.5 m/s, and 9 m/s and the primary/speed of secondary air ratio of 3, 3.5, 4, 4.5, and 5 are selected to conduct the followed numerical simulation.

Figures 6(a) and 6(b) show the velocity effects of the primary and secondary air on the temperature of primary air outlet and the cooling efficiency, respectively. When the primary air speed increases from 6.5-8 m/s, the speed of secondary air is irrespective, the temperature of primary air outlet decreases, and the cooling efficiency increases. When the primary air speed exceeds 8 m/s, it is necessary to determine the speed effects of the primary air according to the speed of secondary air.

When the ratio of the primary air speed to the speed of secondary air increases from 3-4.5, both the speed of secondary air and the temperature of primary air outlet decrease, and the cooling efficiency increases, so, the more reasonable operation point could be the speed of primary air at 8 m/s for the TIEC. The reason should be that when the speed of secondary air decreases from 2.67-1.78 m/s, the reasonable balance point between the sensible heat of the secondary air and the latent heat from the water film evaporation is approached to the heat and mass exchanging sufficiently outside tube. When this ratio rises from 4.5-5, the TIEC performance worsens if overlooking the primary air speed. The reason should be that the speed of secondary air is too slow to keep a larger humidity difference between the secondary air and the water film, which slows the mass transfer along the secondary air path.

Except for the speed ration of 5, the more reasonable operation point of the TIEC should be at the primary air speed of 8 m/s. At the speed ration of 5, the primary air speed of

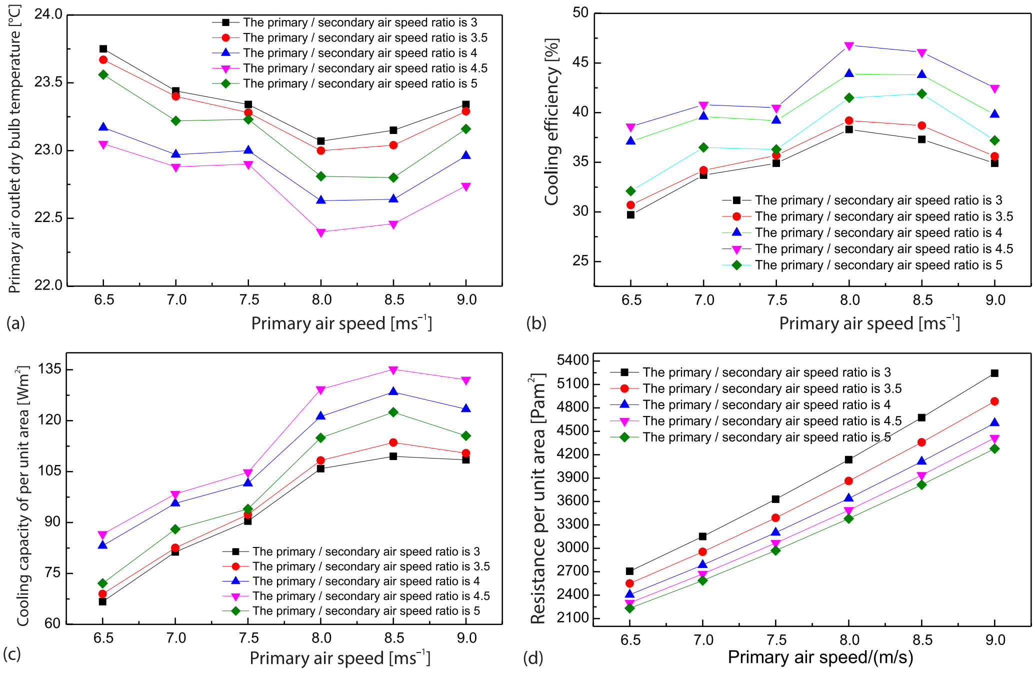

Figure 6. Velocity effects of the primary and secondary air; (a) effects on the temperature of primary air outlet, (b) effects on the cooling efficiency, (c) effects on the cooling capacity, and (d) effects on the resistance

9 m/s and the speed of secondary air of 1.4 m/s should be the more reasonable combination than 8 m/s and 1.6 m/s. When the air speed increases more, the heat and mass transfer of the air could be restricted, because more sensible heat of the air needs to be balanced and the water film outside tube could be destroyed.

Figure 6(c) shows the air speed effects on the cooling capacity per unit area, among of which, the speed of primary/secondary air ratio of 4.5 is the more reasonable condition. When the primary air speed increases from 8.0-8.5, although the cooling capacity continuously increases to a maximum, the primary air quality decreases because its temperature increases. Figure 6(d) shows that the whole air resistance of the TIEC increases linearly with the increase of air speed whether for the primary air or the secondary air.

From the previously mentioned, when the reasonable operation conditions are provided for the discussed TIEC, which are 8 m/s as the primary air speed, 4.5 as the ratio of the primary air speed to the secondary air, 26.1 °C as the environment temperature and 49.04 %RH as the environment humidity, the temperature of primary air outlet is 22.4 °C, the cooling efficiency is 46.8%, the cooling capacity is 128.43 W/m^2, and the resistance per unit area is 3489 Pa/m^2.

Effects of environment parameters

The TIEC performance is heavily depend on environmental parameters, especially humidity. Lanzhou city located in the northwest of China, whose temperature is usually about 30 °C and humidity is usually about 50 %RH in summer. According to the metrological data of Lanzhou in three years, the environment temperature of 28 °C, 29 °C, 30 °C, 31 °C, 32 °C, 33 °C, and 34 °C and the environment humidity of 45 %RH, 50 %RH, 55 %RH, 60 %RH, and 65 %RH are selected, respectively in this paper to do the numerical simulation based on the primary air velocity of 8m/s and the primary/secondary air velocity ratio of 4.5.

Figure 7(a) shows the effect of the environment temperature and humidity on the temperature of primary air outlet, which is identical with common sense. Among the discussed environment humidity conditions, the temperature of primary air outlet is the lowest one when the environment humidity is 45 %RH. When the environment humidity decrease 1 %RH, the the environment humidity decrease 1 %RH, the temperature of primary air outlet decrease about 0.15 °C, and when the environment temperature increase 1 °C, the temperature of primary air outlet increase about 1.01 °C.

Based on figs. 7(b) and 7(c), the environment temperature of 29 °C is the better condition. At this condition, the temperatures of primary air outlet are 23.88 °C, 24.53 °C, 25.3 °C, 26.08 °C, and 26.78 °C, respectively, corresponding to the environment humidity of 45 %RH, 50 %RH, 55 %RH, 60 %RH, and 65 %RH, respectively. Because the result is similar with the section 4.2.1, the whole air resistance of the TIEC is not considered in this section.

In summary, it has more advantages if the environmental parameters are lower for the TIEC mentioned in this paper. When the temperature and humidity are 29 °C and 45 %RH of operation conditions, the temperature of primary air outlet is 23.88 °C and the cooling efficiency is 54.99%.

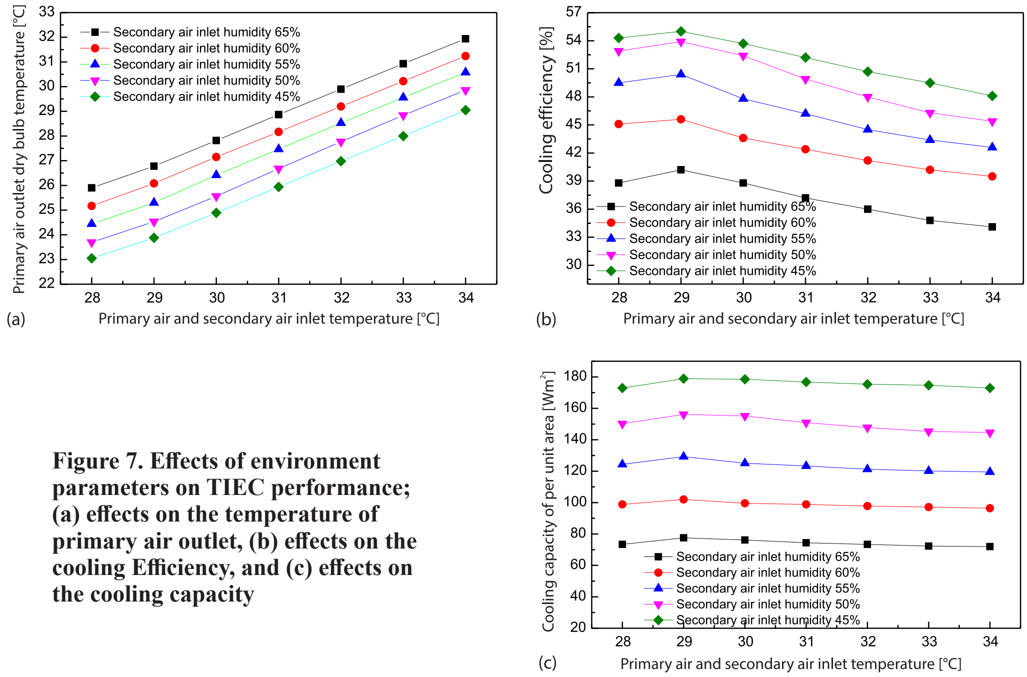

Figure 7. Effects of environment parameters on TIEC performance; (a) effects on the temperature of primary air outlet, (b) effects on the cooling Efficiency, and (c) effects on the cooling capacity

Effects of TIEC structure parameters

Pass length effects of primary and secondary air

At the beginning, because the latent heat from water evaporation is higher than the sensible heat from the secondary air along its pass length, both the temperatures of the water film and the secondary air decrease. Then, with the increase of pass length of the secondary air, the temperature of the water film rises gradually because the water evaporation rate decreases and the latent heat from of water evaporation is less than the sensible heat of the primary air. Meantime, the secondary air resistance increases. It is the same for the primary air, firstly, the primary air temperature decrease, and then, with the increase of the pass length, the heat transfer between the primary air and the tube wall will decrease due to the gradual decrease of temperature difference of both. Simultaneously, the primary air resistance increases. Thus, it is necessary to determine the reasonable pass length of the primary air and the secondary air for the cooling capacity and operation parameters predetermined. For this purpose, the primary air pass length of 1.3 m, 1.4 m, 1.5 m, 1.6 m, 1.7 m, and 1.8 m and the secondary air pass length of 1.18 m, 1.3 m, 1.4 m, 1.5 m, and 1.6 m are selected. Figure 8 shows the numerical results based on the primary air velocity of 8 m/s, the primary/secondary air velocity ratio of 4.5, the environment temperature of 29 °C and the environment humidity of 45%.

According to figs. 8(a)-8(c), the combination of the primary air pass length of 1.5 m and the secondary air pass length of 1.4 m is superior for the TIEC mentioned in this paper. With this pass length, the temperature of primary air outlet, the cooling efficiency and the cooling capacity are 23.31 °C, 61.12%, and 198.77 W/m^2, respectively. When the primary air pass length is longer than 1.5 m, the outlet temperature of the primary air decreases gently with the pass length, and the cooling efficiency and cooling capacity per unit area all decreases because the temperatures of primary air outlet and the heat transfer area increase.

When the pass length expands, the combination effect of the strengthen of both the air resistance and the heat transfer area waken the resistance per unit area, which is shown in fig. 8(d). The resistance per unit area is 3655 Pa/m^2 when the pass lengths of the primary air and the secondary air are 1.5 m and 1.4 m, respectively.

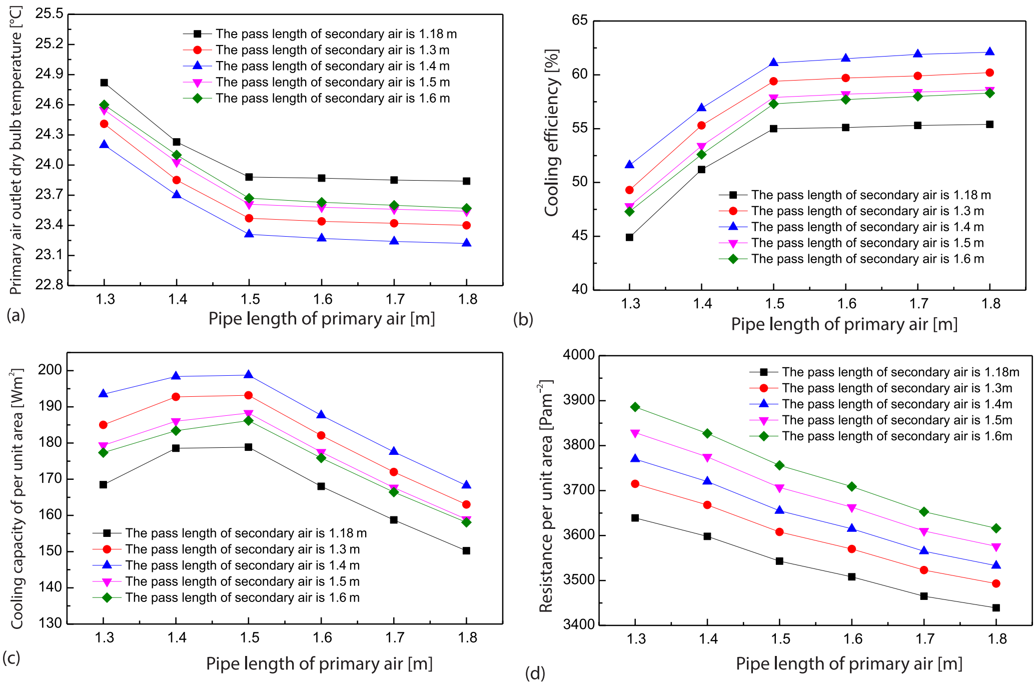

Figure 8. Pass length effects of primary and secondary air; (a) effects on the temperature of primary air outlet, (b) effects on the cooling efficiency, (c) effects on the cooling capacity, and (d) effects on the resistance

Effects of pipe diameter and pipe spacing

When the hydraulic diameter and the velocity are constant, with the extension of relative pipe spacing, the water film will evaporate more and faster at first due to more second air introduced, which lead to the decrease of primary air temperature and the improvement of cooling capacity. Then, the water evaporation will tend to the maximum if the relative pipe spacing is increased continually. Similarly, with the hydraulic diameter increasing at the constant pipe spacing and velocity, the heat transfer would be improved originally due to the escalation of the water film area and the heat transfer area. Then, the primary air temperature and the cooling capacity may decrease because more primary air couldn't be cooled enough, and the evaporation will change if the hydraulic diameter is increased continually. Therefore, there should be a reasonable combination of the hydraulic diameter and the relative pipe spacing for a certain TIEC. To obtain this solution, the relative pipe spacings of 1.3 m, 1.5 m, 1.7 m, 1.9 m, 2.1 m, and 2.3 m and the hydraulic diameters of 0.011 m, 0.017 m, 0.022 m, 0.027 m, and 0.032 m are selected to operate the numerical simulation.

Figure 9(a)-9(c) show the effects of the hydraulic diameter and the relative pipe spacing on the primary air temperature, the cooling efficiency and the cooling capacity, respectively. The indication by the fig. 9 is identical with the aforementioned analysis. When the relative pipe spacing is more than 1.7 m, the continuous escalation of the relative pipe spacing continually has limited impact on improving heat transfer. When the hydraulic diameter is more than 0.022 m, it is disadvantageous to improve heat transfer by increasing the hydraulic diameter unceasingly. Figure 9(d) shows the whole air resistance of the TIEC, which reinforce proportionally corresponding to the hydraulic diameter decreasing, and weaken insignificantly with the relative pipe spacing increasing.

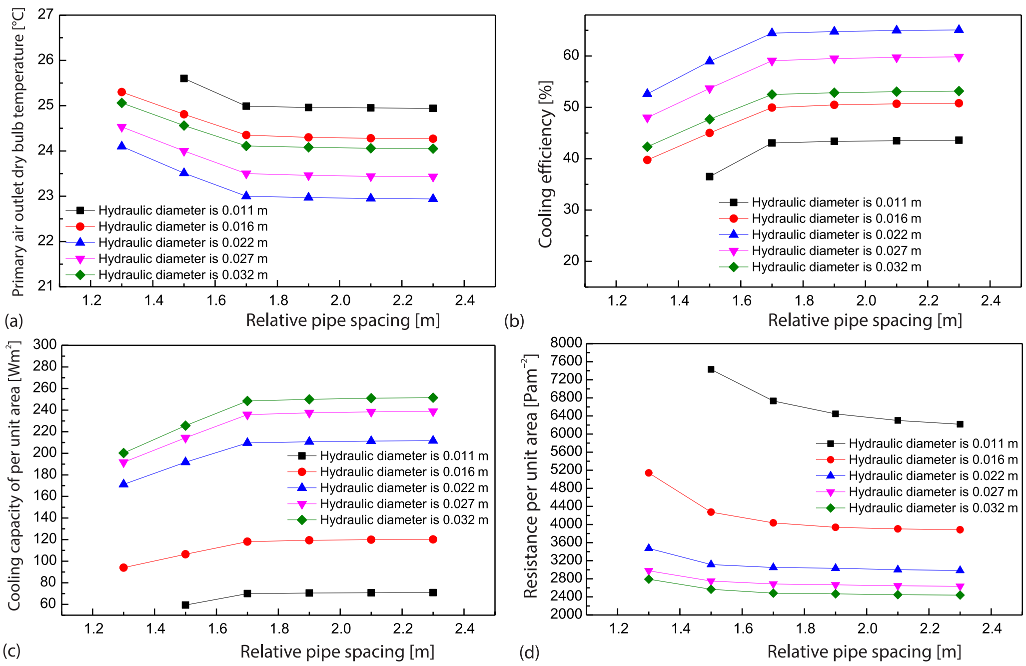

Figure 9. Effects of the pipe diameter and the pipe spacing; (a) effects on the temperature of primary air outlet, (b) effects on the cooling efficiency, (c) effects on the cooling capacity, and (d) effects on the resistance

According to figs. 9(a)-9(d), the hydraulic diameter of 0.022 m and the relative pipe spacing of 1.7 m could be the appropriate structure for the TIEC mentioned in the paper. In this condition，the temperature of primary air outlet, the cooling efficiency, the cooling capacity per unit area and the resistance per unit area are 23.01 °C, 64.34%, 209.6 W/m^2, and 3015 Pa/m^2, respectively.

Conclusions

In this paper, a 3-D numerical model and method of TIEC, which is based on the conservation equation, standard k-ε model, VOF model and the test data, is obtained and verified. Then, the effects of the working parameters and the structure parameters on the TIEC performance are analyzed by the SIMPLE algorithm, the evaporation UDF model and FLUENT software. The conclusions are obtained as follow.

- The 3-D full-scale numerical model and method of TIEC built in this paper are reliable and effective.
- In the operation conditions of the paper, the primary air pass length of 1.5 m, the secondary air pass length of 1.4 m, the hydraulic diameter of 0.022 m and the relative pipe spacing of 1.7 m are reasonable, and the primary air speed of 8 m/s, the primary/speed of secondary air ratio of 4.5 are recommended.

Nomenclature

A_p – heat transfer area of on-way resistance of primary air, [m^2]
$A_{p'}$ – heat transfer area of local resistance of primary air, [m^2]
A_s – heat transfer area of secondary air, [m^2]
C_f – row number of secondary air-flow direction
c – average specific heat capacity of primary air, [Jkg^{-1}°C^{-1}]
$G_{\max}$ – mass velocity of secondary air at minimum section, [kgm^{-}2s^{-1}]
g – gravitational acceleration, [ms^{-2}]
h – convective transfer coefficient, [kgm^{-2}s^{-1}]
i – specific enthalpy, [kJkg^{-1}]
k – thermal conductivity, [Wm^{-1}K^{-1}]
k_D – mass transfer coefficient, [kgm^{-}2s^{-1}]
L – hydraulic diameter of pipe, [m]
l – pipe length, [m]
M – mass of liquid droplets evaporated into gas droplets, [kg]
m – mass-flow rate, [kgm^{-1}s^{-1}]
n – the number of tube
p_p – on-way resistance per unit area of primary air, [Pam^{-2}]
$p_{p'}$ – local resistance per unit area of primary air, [Pam^{-2}]
p_s – resistance per unit area of secondary air, [Pam^{-2}]
S_ϕ – source term
T – temperature, [°C]
T_{wb} – wetbulb temperature, [°C]
T_q – saturated droplet temperature, [°C]
t – time
u – air speed, [ms^{-1}]
W – specific humidity, [kgkg^{-1}]

Geek symbols

ρ – density of microelements, [kgm^{-3}]
μ – dynamic viscosity, [Pas^{-1}]
ζ – local resistance coefficient
ϕ – general variable
λ – drag coefficient
Γ_ϕ – diffusion coefficient

Subscripts

1 – primary air
1′ – inlet of primary air
1″ – outlet of primary air
2 – secondary air
f – water film
fg – latent heat
ℓ – liquid droplet
w – tube wall
x – x-direction
y – y-direction
z – z-direction

References

[1] Dodoo, A., *et al*., Building Energy-Efficiency Standards in a Life Cycle Primary Energy Perspective, *Energy and Buildings*, *43* (2011), 7, pp. 1589-1597

[2] Wang, L., *et al*., The Energy and Exergy Analysis on the Performance of Counter-Flow Heat and Mass Exchanger for M-Cycle Indirect Evaporative Cooling, *Thermal Science*, *23* (2019), 2A, pp. 613-623
[3] Chen, Q., *et a*l., A New Approach to Analysis and Optimization of Evaporative Cooling System I: *Theory Energy*, *35* (2010), 6, pp. 2448-2454
[4] Chen, Q., *et al*., A New Approach to Analysis and Optimization of Evaporative Cooling System II: *Applications Energ*y, *36* (2011), 2, pp. 2890-2898
[5] Duan, Z., *et al.*, Indirect Evaporative Cooling: Past, Present and Future Potentials, *Renewable & Sustainable Energy Reviews, 16* (2012), 9, pp. 6823-6850
[6] Zhou, Y., *et al*., Numerical Study and Optimization of a Combined Thermoelectric Assisted Indirect Evaporative Cooling System, *Journal of Thermal Science*, *29* (2020), 5, pp. 1345-1354
[7] Hettiarachchi, H. D., *et al*., The Effect of Longitudinal Heat Conduction in Cross-Flow Indirect Evaporative Air Coolers, *Applied Thermal Engineering*, *27* (2007), 1112, pp. 1841-1848
[8] Yunran, M., *et al*., Simplified Predicting Models on Energy-Saving Potential of Indirect Evaporative Coolers in Hong Kong, *Energy Procedia*, *159* (2019), Feb., pp. 225-230
[9] Zheng B., *et a*l., Development of an Experimental Validated Model of Cross-Flow Indirect Evaporative Cooler with Condensation, *Applied Energy*, *252* (2019), 113438
[10] Chen, Y., *et al*., A Simplified Analytical Model for Indirect Evaporative Cooling Considering Condensation from Fresh Air: Development and Application, *Energy and Building*s, *108* (2015), Dec., pp. 387-400
[11] Chengqin, R., Hongxing, Y., An Analytical Model for the Heat and Mass Transfer Processes in Indirect Evaporative Cooling with Parallel/Counter Flow Configurations, *International Journal of Heat and Mass Transfer*, *49* (2006), 34, pp. 617-627
[12] Moshari, S., *et al.*, Numerical Investigation of Wet-Bulb Effectiveness and Water Consumption in one- and Two-Stage Indirect Evaporative Coolers, *Energy Conversion and Management*, *108* (2016), Jan., pp. 309-321
[13] Cui, X., *et al.*, Fundamental Formulation of a Modified LMTD Method to Study Indirect Evaporative Heat Exchangers, *Energy Conversion and Management*, *88* (2014), Dec., pp. 372-381
[14] Hao, L., Experimental Study on Indirect Tube Type Evaporative Cooler and Temperature Simulation, Ph. D. thesis, Lanzhou Jiaotong University, Lanzhou, China, 2013
[15] Min, Y., *et al*., A Statistical Modelling Approach on the Performance Prediction of Indirect Evaporative Cooling Energy Recovery Systems, *Applied Energy*, *255* (2019), 113832
[16] Min, Y., *et al.*, Numerical Study on Indirect Evaporative Coolers Considering Condensation: A thorough Comparison between Cross-Flow and Counter Flow, *International Journal of Heat and Mass Transfer*, *131* (2019), 6, pp. 472-486
[17] Sun, T., *et a*l., Theoretical and Experimental Study on Heat and Mass Transfer of a Porous Ceramic Tube Type Indirect Evaporative Cooler, *Applied Thermal Engineering*, *173* (2020), 115211
[18] Porumb, B., *et a*l., A Review of Indirect Evaporative Cooling Technology, *Energy Procedia*, *85* (2016), Jan., pp. 461-471
[19] Anisimov, S., *et al*., Performance Investigation of a M (Maisotsenko)-Cycle Cross-Flow Heat Exchanger Used for Indirect Evaporative Cooling, Energy, *76* (2014), Nov., pp. 593-606
[20] Pandelidis, D., *et al*., Counter-Flow Indirect Evaporative Cooler for Heat Recovery in the Temperate Climate, *Energy*, *165* (2018), Sept., pp. 877-894
[21] Halasz, B., A General Mathematical Model of Evaporative Cooling Devices (in French), *Revue générale de thermique*, *37* (1998), 4, pp. 245-255
[22] Riangvilaikul, B., Kumar, S., An Experimental Study of a Novel Dew Point Evaporative Cooling System, *Energy and Buildings*, *42* (2010), 5, pp. 637-644
[23] Gholamalizadeh, E., *et al*., Study of Intensification of the Heat Transfer in Helically Coiled Tube Heat Exchangers Via Coiled Wire Inserts, *International Journal of Thermal Science*s, *141* (2019), July, pp. 72-83
[24] Yu, K., Experimental Study on Heat Transfer Characteristics of Tubular Indirect Evaporative Cooler, Ph. D. thesis, Lanzhou Jiaotong University, Lanzhou, China, 2014

Paper submitted: November 21, 2020
Paper revised: May 14, 2021
Paper accepted: May 16, 2021